Zeitschrift: Technische Mitteilungen / Schweizerische Post-, Telefon- und Telegrafenbetriebe = Bulletin technique / Entreprise des postes, téléphones et télégraphes suisses = Bollettino tecnico / Azienda delle poste, dei telefoni e dei telegrafi svizzeri

Herausgeber: Schweizerische Post-, Telefon- und Telegrafenbetriebe

Band: 55 (1977)

Heft: 2

Artikel: Eart station antenna using : a corrugated horn-reflector feed

Autor: Sato, Ikuro / Sarkar, Subrata K.

DOI: https://doi.org/10.5169/seals-874118

Nutzungsbedingungen

Die ETH-Bibliothek ist die Anbieterin der digitalisierten Zeitschriften. Sie besitzt keine Urheberrechte an den Zeitschriften und ist nicht verantwortlich für deren Inhalte. Die Rechte liegen in der Regel bei den Herausgebern beziehungsweise den externen Rechteinhabern. Siehe Rechtliche Hinweise.

Conditions d'utilisation

L'ETH Library est le fournisseur des revues numérisées. Elle ne détient aucun droit d'auteur sur les revues et n'est pas responsable de leur contenu. En règle générale, les droits sont détenus par les éditeurs ou les détenteurs de droits externes. Voir Informations légales.

Terms of use

The ETH Library is the provider of the digitised journals. It does not own any copyrights to the journals and is not responsible for their content. The rights usually lie with the publishers or the external rights holders. See Legal notice.

Download PDF: 13.05.2025

ETH-Bibliothek Zürich, E-Periodica, https://www.e-periodica.ch

Earth Station Antenna Using

A Corrugated Horn-Reflector Feed

Ikuro SATO, Tokyo, and Subrata K. SARKAR, Berne

621.396.677.73:621.396.934:629.783

Summary. *This report presents details of the configuration and RF performance of Leuk earth station antenna using a corrugated horn-reflector primary feed, along with its design background and analysis. The conical section of the horn-reflector was corrugated to improve radiation properties. Theoretical and experimental studies of its electrical performance were undertaken. The corrugated horn-reflector was employed as a primary feed of 97 ft cassegrain antenna constructed at Leuk earth station in 1973. The antenna has been operating in the Atlantic region with the Intelsat system since January 1974. It was confirmed that the corrugated horn-reflector feed improved the aperture efficiency, noise temperature and cross polarization characteristics.*

1 Introduction

Since the epoch-making launching of the first commercial communications satellite – "Early Bird" – in 1965, satellite telecommunication has experienced rapid growth every year. At the end of 1973, 87 antennas at 69 earth station sites in 52 different countries carry a number of telephone, telegraph and television messages through the five Intelsat IV satellites in orbit, thus completing the global satellite communications network.

For the antenna system, a near field cassegrain antenna fed by a horn-reflector has been widely used in these earth stations. From a standpoint of operation and maintenance, this type of antenna has the advantage of allowing communication equipments to be installed in a position independent of the antenna elevation angle. The horn-reflector feed possesses also electrical advantages of broadband and low noise characteristics because of its plane wavefront aperture. Such the near field cassegrain antenna [1] has been improved and widely accepted in many commercial earth stations.

However, the asymmetrical radiation pattern of the conventional horn-reflector gives degraded aperture efficiency and noise temperature.

For future frequency reuse systems, using dual orthogonal polarization, the conventional feed produces large unacceptable cross polarization components.

On the other hand, the use of dual-mode [2] or hybrid mode [3] feed has been suggested to improve the radiation performances of primary feed including cross polarization.

As a method of improving the above-mentioned defects of the conventional horn-reflector, it is an excellent idea to replace a conical section of the horn-reflector with a corrugated conical horn.

Prior to the construction of the full-size corrugated horn-reflector, the model studies of its electrical characteristics were undertaken, and the corrugated horn technique proved a great success.

The radiation performances of the corrugated horn-reflector were confirmed through the full-size measurements and theoretical studies.

The corrugated horn-reflector was employed as a primary feed of 97 ft cassegrain antenna constructed in 1973 at Leuk earth station.

This paper describes design philosophy, general configuration and performance of the cassegrain antenna and then discusses some details of the corrugated horn-reflector feed.

2 Antenna Feed System Design Philosophy

The satellite communication earth station antenna is generally required not only to assure high electrical performances such as the figure of merit (G/T) and gain and noise temperature, but also to possess advantages of operation and maintenance.

The horn-reflector is suitable for primary feed of the yoke-and-tower type near field cassegrain antenna, since this feed has the following features:

- Communication equipments can be installed on the floor independent of antenna elevation angle change.
- Cassegrain subreflector can be operated in near field region of the primary feed. This contributes to the electrical broadband and low noise capability.

The horn-reflector feed has been widely used in the near field cassegrain antenna because of these features.

However, it should be pointed out that there are considerable problems as to the improvement of pattern symmetry. The conventional horn-reflector exhibits a large amount of ripple in E-plane radiation pattern. This defect not only degrades the antenna aperture efficiency and noise temperature characteristics but also limits the effects of shaping technique of cassegrain profile. Furthermore, the inferior cross polarization characteristics of this feed will cause a serious problem to future frequency reuse systems using dual orthogonal polarization.

If the corrugated horn technology is applied to the horn-reflector, the radiation performance is considerably improved, and the yoke-and-tower type near field cassegrain antenna will become more attractive, remaining the favorable feature in operation and maintenance.

For development of the new antenna, special attention must be paid also to the supporting structure of the subreflector, that is, the subreflector must be supported by symmetrical quadripod, considering the cross polarization products.

It is a matter of course that the maximum figure of merit (G/T) must be attained for the specified main reflector diameter and sufficient operational margin must be kept. The antenna gain (aperture efficiency) and noise temperature should be optimized by analyzing the diffraction field of the subreflector from the viewpoint of electromagnetic diffraction theory.

3 Feed System Configuration

31 General Configuration and Performance

Prior to statement of the feed system configuration, the major configuration and design performances of this 97 ft

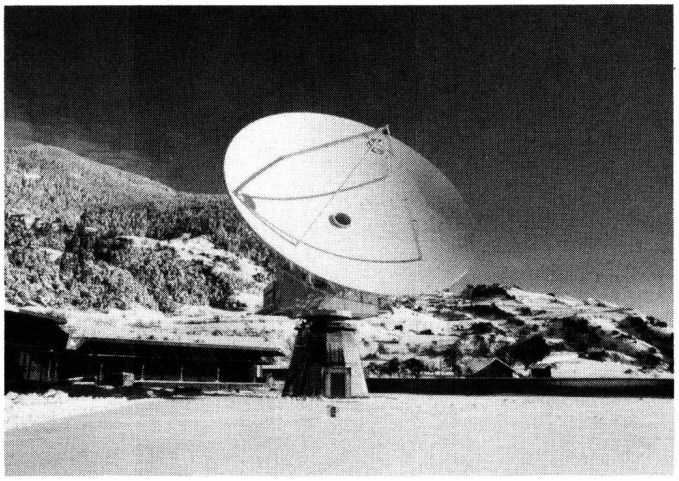

Fig. 1
Leuk earth station antenna

cassegrain antenna are outlined as follows. A photograph of this antenna is shown in *Figure 1*.

Antenna feed system	Corrugated horn-reflector (high efficiency shaped reflector has been adopted)
Autotracking system	Monopulse, mode tracking system with wideband mode-coupler covering 3.7 to 4.2 GHz
Diameter and F/D	97 ft in diameter, F/D = 0.36
Surface accuracy	E/D less than 4×10^{-5}. (E is rms pathlength error due to surface inaccuracy)
Antenna mount	Elevation over azimuth
Polarization	Circular
Drive system	SCR controlled electric motor drive, dual train antibacklash
Locked rotor natural frequency	More than 2.2 Hz
Beacon frequency selection	Two or more. Predetermined frequencies are remotely selectable from the ACC
Gain	More than 60.0 dB at 4.0 GHz
G/T	More than 41.8 dB/K at 4 GHz at 5° elevation
Sky coverage	AZ: ±170° EL: 0°–92°

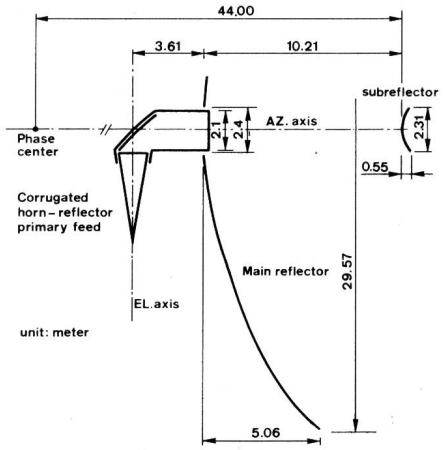

Fig. 2
Cassegrain geometry of 97 ft antenna

32 Cassegrain Geometry

The 97 ft cassegrain antenna geometry is decided by high efficiency shaped reflector technique and diffraction field analysis from the subreflector, using the experimented patterns of the primary feed model-scaled to 0.375.

Figure 2 shows the cassegrain geometry of the 97 ft antenna. The profile of the subreflector is shaped to give a nearly uniform distribution over the main reflector aperture for an illumination taper of about –17 dB at the subreflector edge. The resultant phase errors introduced by the profile shaping are removed by slightly changing the main reflector from parabolic curve of 10,668 mm focal length. The phase center is positioned at 44 m from the subreflector vertex to minimize the residual phase error. This position is decided from the measurement results of the phase patterns of the corrugated horn-reflector feed.

The subreflector is made from glass fibre reinforced epoxy resin, and the reflecting surface is coated with flame sprayed aluminium.

To prevent the accumulation of snow and the formation of ice, the electric de-icing systems are furnished to the main reflector panels, the subreflector and its supporting rods.

The subreflector is supported by a quadripod structure, whose electrical symmetry contributes to minimum cross polarization products.

33 Corrugated Horn-Reflector Primary Feed

The corrugated horn-reflector primary feed consists of a corrugated conical horn, an offset paraboloidal reflector and shielding duct.

The operational principle can be explained by geometrical optics. *Figure 3* provides the configuration of the primary feed. The apex of the conical horn coincides with the focus of the paraboloid, and the axis of the horn is perpendicular to the axis of the paraboloid. The paraboloidal reflector acts as phase corrector for the diverging spherical wavefront from the conical horn, so that the wave appearing at the circular aperture has a plane wavefront.

The primary feed rotates with the cassegrain reflectors around the conical horn axis coincident with the antenna elevation axis. The corrugated conical horn is connected, through an elevation rotary joint, to the composite feed on the stationary floor.

The shielding duct encircles the circular aperture as well as the paraboloidal reflector and the corrugated horn aperture, and contributes to low noise characteristics.

The corrugated horn is fabricated from aluminium and its aperture is covered with an electrically transparent dielectric sheet. In order to keep the surface of feed horn cover dry and

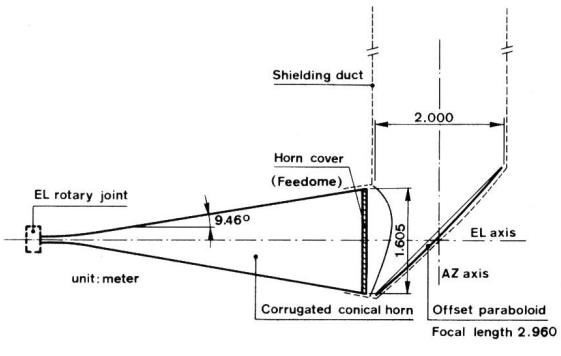

Fig. 3
Configuration of corrugated horn-reflector feed

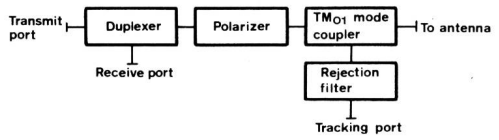

Fig. 4
Block diagram of composite feed

clean, a rain blower is provided. The de-icing heater panels are stuck over the back surface of the reflector to prevent the accumulation of snow and the formation of ice.

34 Composite Feed

The composite feed should be designed in accordance with the following criteria.

- Beacon frequency may be allocated in any frequency within the receive band.
- Circular polarization is used for tracking.
- The composite feed insertion loss must be minimized to give a good G/T.

The composite feed is composed of a mode coupler, a polarizer and a duplexer with a rejection filter. This is characterized by the 2-channel monopulse mode tracking system, using the broadband TM_{01} mode coupler as a tracking error signal probe. *Figure 4* shows a block diagram of the designed composite feed and *Table I* shows the performance summary.

Table I. Improved composite feed performance

Frequency band Performance	Receive band	Transmit band
Insertion loss	Less than 0.15 dB	Less than 0.15 dB
VSWR	Less than 1.2	Less than 1.3
Axial Ratio (circular polarization)	Less than 2 dB	Less than 2 dB
Isolation between receive and transmit port at 6 GHz	More than 80 dB	
Isolation between transmit and difference port	More than 80 dB	

4 Corrugated Horn-Reflector Analysis

41 Introduction

The radiation pattern of the corrugated horn-reflector can be computed by applying the *Kirchhoff* approximation to the aperture excited by hybrid mode of the corrugated waveguide. The full-size measurements were performed in plant to verify the model studies and theoretical analysis.

The primary patterns of the corrugated horn-reflector feed are compared with those of the conventional horn-reflector feed. These studies indicate that the corrugated horn technique improves the electrical performances of the horn-reflector, and this primary feed is highly desirable for the near field cassegrain antenna.

42 Radiation Calculation

The radiation pattern from the corrugated horn-reflector can be computed by applying the Kirchhoff approximation to

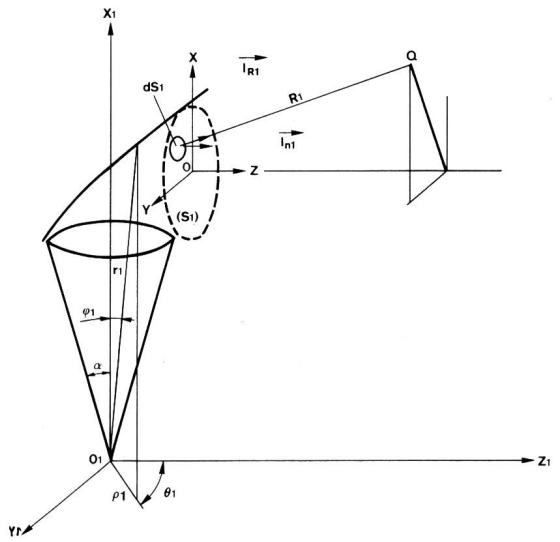

Fig. 5
Coordinates of corrugated conical horn-reflector

the reference aperture S_1. Referring *Figure 5*, electric field $\vec{E}_{s1}$ at observing point Q is given as follows [4]:

$$\vec{E}_{s1} = \frac{j}{2\lambda}\int\int_{(S_1)} [\vec{E}_{a1}(1+\vec{I}_{n1}\cdot\vec{I}_{R1}) - (\vec{E}_{a1}\cdot\vec{I}_{R1})(\vec{I}_{n1}+\vec{I}_{R1})]\cdot \frac{e^{-jkR_1}}{R_1}\, dS_1 \quad (1)$$

where, k is free-space wave number.

If $(\vec{E}_{a1})_x$ and $(\vec{E}_{a1})_y$ are the aperture components, then at point Q, the components $(\vec{Es}_1)_x$ and $(\vec{Es}_1)_y$ are as follows:

$$\begin{bmatrix}(\vec{E}_{s1})_x \\ (\vec{E}_{s1})_y\end{bmatrix} = \frac{j}{2\lambda}\int\int_{S_1}\begin{bmatrix}(\vec{E}_{a1})_x \\ (\vec{E}_{a1})_y\end{bmatrix}\cdot F_1(x,y,X_1,Y_1,Z_1)\, dS_1, \quad (2)$$

where

$$F(x,y,X_1,Y_1,Z_1) = \frac{e^{-jkZ_1}}{Z_1}\cdot e^{-jk(X_1^2+Y_1^2)}\cdot e^{-jk(x^2+y^2)/2Z_1}\cdot e^{jk(xX_1+yY_1)/Z_1} \quad (3)$$

$$x = 2fp\cos\eta - 2f(\sqrt{p_0^2+1} - \sqrt{p^2+1}),\ y = 2fp\sin\eta \quad (4)$$

$$\tan\eta = \sin\Theta_1\cos\varphi_1/(\cos\Theta_1 - \sin\varphi_1) \quad (5)$$

$$dS_1 = (2f)^2 p\left(1 + \frac{p}{\sqrt{p^2+1}}\cos\eta\right) dp\, d\eta \quad (6)$$

$$p = \tan\varphi_1,\ p_0 = \tan\alpha \quad (7)$$

In the corrugated horn-reflector, after reflection from the offset parabola, the polar field components in the circular corrugated waveguide transform conformally into the corresponding bipolar components in the aperture plane.

Considering the attenuation due to path length differences the components are as follows [5]:

$$(\vec{E}_{a1})_x = \frac{2f}{r_1}(E_{\varrho 1}\cos\eta + E_{\Theta 1}\sin\eta) \tag{8}$$

$$(\vec{E}_{a1})_y = \frac{2f}{r_1}(E_{\varrho 1}\sin\eta - E_{\Theta 1}\cos\eta) \tag{9}$$

In the above equations, f is focal length of the paraboloidal reflector, and α is half flare angle of the conical horn.

In the above equations, $E_{\varrho 1}$ and $E_{\Theta 1}$ are given as the radial and circumferential field components of the hybrid dominant mode in a circular corrugated waveguide, assuming that the corrugation pitch and teeth of the corrugated circular waveguide are sufficiently small compared with the free space wavelength and that the space harmonics and higher modes inside the corrugation are neglected [6].

$$E_{\varrho 1} = E_0\left\{J_1'(\sigma\varrho_1) + t\sigma b\frac{J_1(\sigma\varrho_1)}{\sigma\varrho_1}\right\}\begin{pmatrix}\cos\Theta_1\\ \sin\Theta_1\end{pmatrix} \tag{10}$$

$$E_{\Theta 1} = E_0\left\{\frac{J_1(\sigma\varrho_1)}{\sigma\varrho_1} + t\sigma b J_1'(\sigma\varrho_1)\right\}\begin{pmatrix}-\sin\Theta_1\\ \cos\Theta_1\end{pmatrix} \tag{11}$$

where

$$t = -\frac{J_1'(\sigma b)}{J_1(\sigma b)} \tag{12}$$

and σb is given by the characteristic equation for the hybrid mode in a corrugated waveguide.

For the purpose of calculation of conventional horn-reflector, the value of $t = 0$ can be rewritten in Eqs. (10) and (11), that is, $\sigma b = 1.841$ is inserted.

The co-polarized and cross polarized radiation patterns of the horn-reflector feed were numerically calculated in accordance with the configuration shown in Figure 3.

The calculated patterns near the subreflector at 3.950 MHz and 6.175 MHz are shown in Figures 6 and 7, comparing with the case of the conventional horn-reflector.

Figure 6 shows the co-polarized radiation patterns, and indicates that the beam symmetry is comfortably improved by corrugating the conical horn. *Figure 7* shows the cross polarized radiation patterns, and indicates that the beam peak of cross polarization is about 28 dB below the co-polarization peak, that is, more than 10 dB improvement by corrugation technique.

43 Radiation Measurement

A full-size corrugated horn-reflector was constructed in order to verify the cassegrain antenna performances estimated by the model scaled studies and the theoretical analysis. *Figure 8* shows the practical setup of this horn-reflector feed in plant.

Figure 9 shows measured radiation patterns of the corrugated horn-reflector feed. A very good agreement has been obtained between the calculated and measured patterns.

The measured phase patterns are plotted in *Figure 10*, together with the theoretical results.

From these full-size measurements, it was confirmed that the electrical performances of the 97 ft antenna designed by the model studies were satisfied.

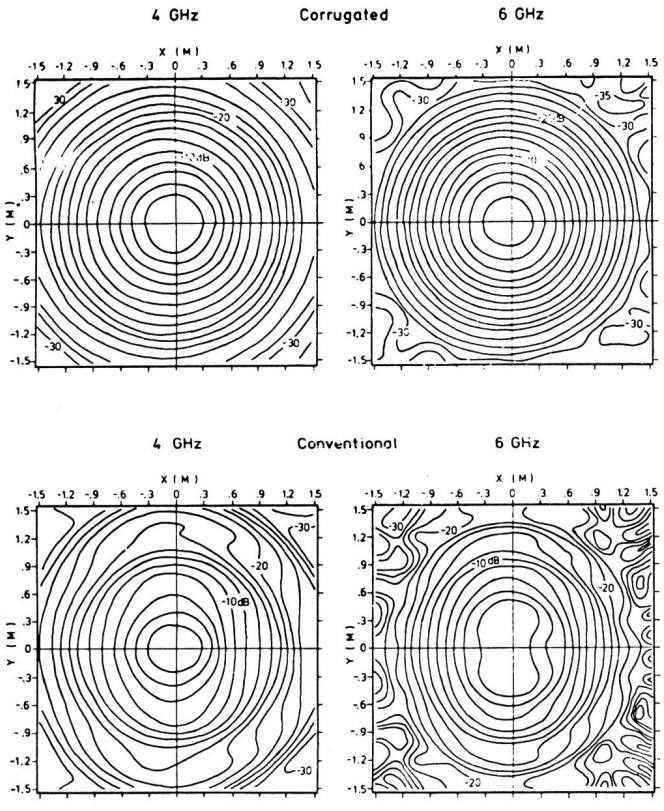

Fig. 6
Conical horn-reflector radiation pattern (calculated, Co-Polarization)

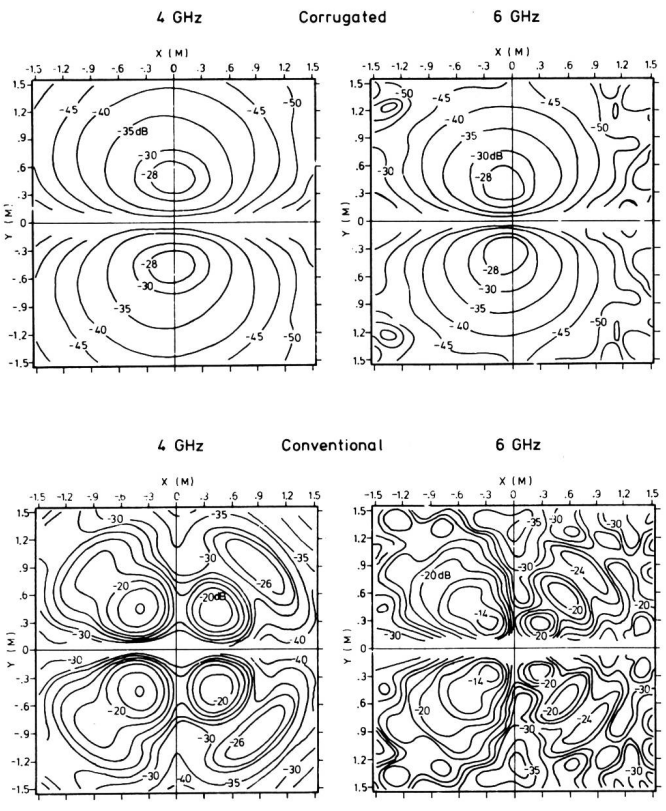

Fig. 7
Conical horn-reflector radiation pattern (calculated, Cross Polarization)

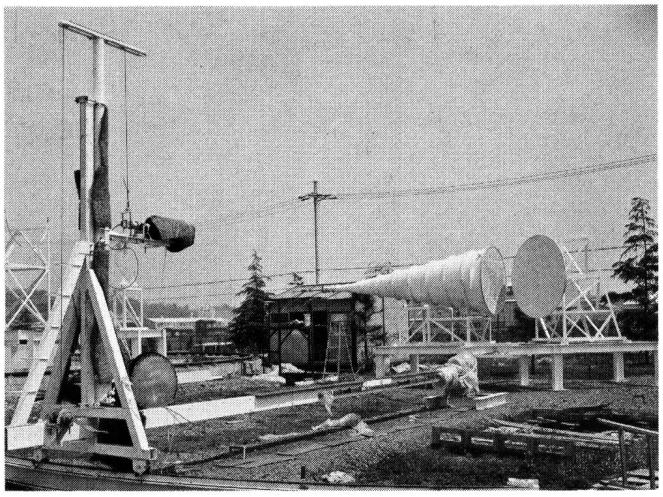

Fig. 8
Full-size experimental setup

5 Antenna Performance Estimation

51 Antenna Efficiency Estimation

Gain G of the aperture type antenna is defined as a function of the aperture area and its efficiency, as follows:

$$G = \eta \frac{4\pi A}{\lambda^2} \tag{13}$$

where A is the cross-sectional area of the antenna aperture, η is the total antenna efficiency and λ is the wavelength.

Accurate calculation of η is fairly complicated, but, for most practical purposes, it is adequate to express η as the following product:

$$\eta = \eta_{ill} \cdot \eta_{sm} \cdot \eta_{ss} \cdot \eta_B \cdot \eta_{tol} \cdot \eta_P \cdot \eta_C \cdot \eta_L \cdot \eta_D \tag{14}$$

These factors are defined as follows:

η_{ill}	Amplitude illumination	Uniformity of the illumination over the antenna aperture
η_{sm}	Spillover from main reflector	Energy spilled from the main reflector
η_{ss}	Spillover from subreflector	Energy spilled from the subreflector
η_B	Blocking and scattering	Shadowing the antenna aperture by the subreflector and its supporting structures
η_{tol}	Surface accuracy	Loss due to the irregularity of the surface of the main reflector, the subreflector and the primary reflector
η_P	Primary phase error	Loss due to the residual phase error of the primary feed
η_C	Cross polarization	Energy contained in the cross polarization components derived from the incompleteness of the composite feed and the reflector geometry
η_L	Feed loss	Total copper loss of the composite feed, the dielectric loss of the feedome and the transmission loss of the corrugated horn
η_D	Diffraction loss of corrugated horn	Coupling loss of corrugated horn and paraboloidal reflector

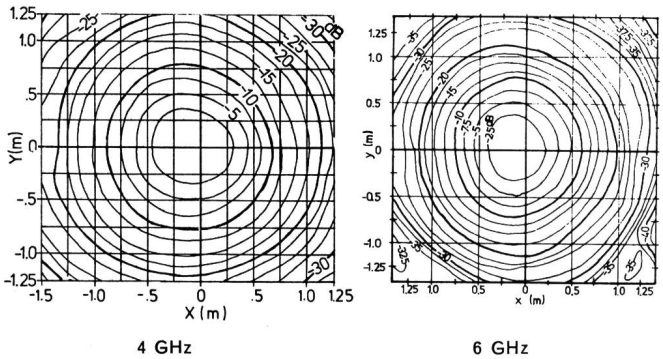

Fig. 9
Measured amplitude pattern

In order to analyze the antenna efficiency, it is necessary to calculate the aperture illumination distribution over the antenna aperture.

For this purpose, it is indispensable to analyze the diffraction field by the subreflector from the viewpoint of electromagnetic diffraction theory.

The scattering pattern from the shaped subreflector is analyzed by a technique involving the vector diffraction theory. It is called the current distribution method.

In order to integrate the current induced on the subreflector, the following is assumed.

- Subreflector diameter is several times larger than the wavelength
- Unit areas on the subreflector are locally plane
- There is no interaction between the primary feed system and the subreflector

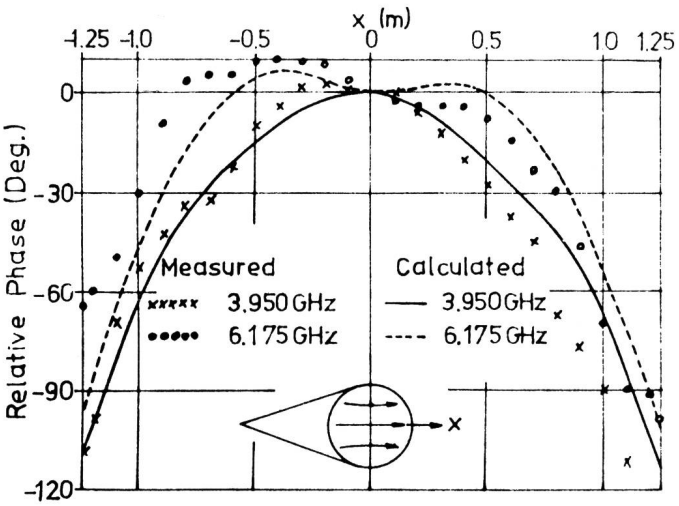

Fig. 10
Phase pattern

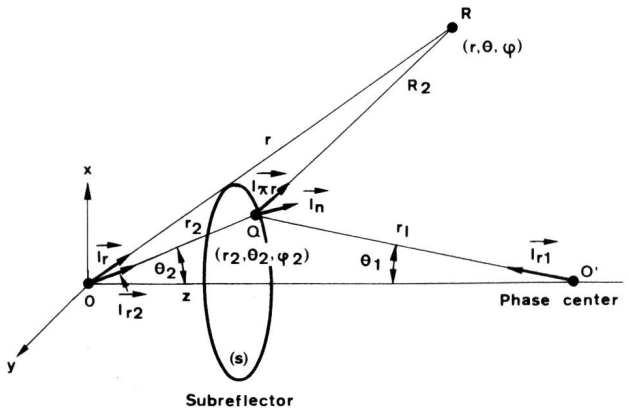

Fig. 11
Coordinate for scattering pattern calculation

Figure 11 shows the subreflector, the coordinates and vector notations to be used in this analysis. Assuming that the system is rotationally symmetric, the scattering field from the subreflector, at an observing point R, is given as follows:

$$\vec{E}_s = -j\frac{\omega\mu}{2\pi}\int\int_S [(\vec{I}_n \times \vec{H}_i) - \{(\vec{I}_n \times \vec{H}_i)\cdot \vec{I}_{\pi r}\}\vec{I}_{\pi r}]$$

$$\times \frac{\exp(-jkR_2)}{R_2} \times \sqrt{1+\left(\frac{dr_2}{r_2 d\Theta_2}\right)^2}\, r_2^2 \sin\Theta_2\, d\Theta_2\, d\varphi_2 \qquad (15)$$

Incident electric field $\vec{E}_i$ on the subreflector is expressed by,

$$\vec{E}_i = \left\{ E_E(\Theta_1)\cos\varphi_1 \vec{I}_{\Theta_1} - E_H(\Theta_1)\sin\varphi_1 \vec{I}_{\varphi_1} \right\} \cdot \frac{\exp(-jkr_1)}{r_1}, \qquad (16)$$

where $E_E(\Theta_1)$ and $E_H(\Theta_1)$ are the radiation patterns of the primary feed system on E- and H-plane, respectively.

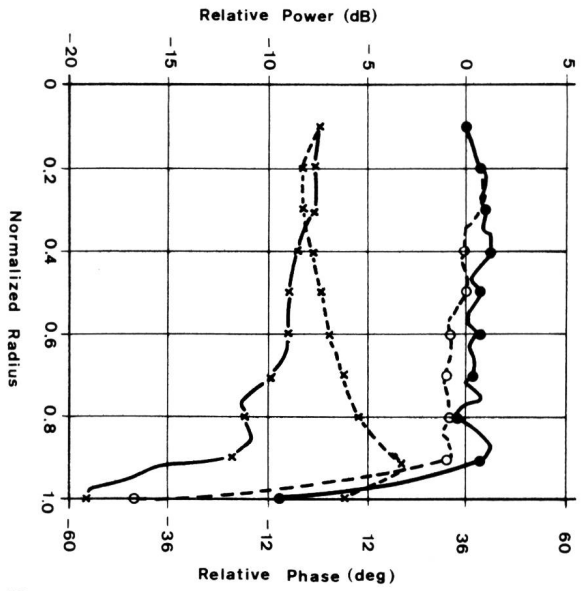

Fig. 12
Aperture field distribution

Amplitude, Phase } 4 GHz

Amplitude, Phase } 6 GHz

From the measured pattern of corrugated horn-reflector primary feed, the field distribution over the antenna aperture was calculated by means of the above-mentioned diffraction theory.

Figure 12 illustrates the aperture field in amplitude and phase, actually calculated by diffraction theory.

From the field distribution over the aperture, efficiency factors such as illumination efficiency, spillover energy from the main reflector, primary phase error and blocking efficiency can be easily estimated.

Table II presents the estimated antenna efficiency by the above-mentioned procedure.

Table II. Estimated antenna efficiency and gain

Frequency	4.000 GHz	6.175 GHz
Feed Loss	0.17 dB	0.18 dB
Reflection Loss	0.04	0.04
Coupling Loss of Corrugated Horn-Reflector	0.03	0.03
Spill-over from Subreflector	0.19	0.05
Spill-over from Main Reflector	0.04	0.01
Illumination Efficiency	0.17	0.24
Blocking and Scattering	0.27	0.27
Residual Phase Error	0.09	0.17
Cross Polarization	0.04	0.04
Surface Accuracy	0.10	0.24
Total Loss	1.14 dB	1.27 dB
100 % Gain of 29.6 m⌀ Antenna	61.86 dB	65.63 dB
Antenna Gain	60.72 dB	64.36 dB

52 Antenna Noise Temperature Estimation

Antenna noise temperature T_A is classified into two categories. One of them is noise, called «external noise», that the antenna will pick up from thermal noise, such as space (galactic noise), atmospheric noise (oxygen and water vapor absorption) and ground noise. The other is noise due to antenna feed loss. These are defined T_{EX} and T_L respectively.

With the atmospheric region, oxygen and water vapor attenuate the radio waves. The atmosphere acts as if it were a microwave attenuator. This phenomenon is called atmospheric absorption [7].

On the other hand, the apparent temperatures of smooth and rough terrain surfaces were calculated by *S.N.C. Chen* and *W.H. Peake* [8]. The ground noise is caused by emissivity and noise estimation is based on measurement of complex dielectric constants for the surface of the earth. It depends upon the condition of the surface, the frequency, the polarization and the scattering parameters.

Antenna noise temperature T_A, given from the external noise source and the feed loss, is formulated as

$$T_A = \frac{T_{EX}}{L} + T_0\left(1 - \frac{1}{L}\right) \qquad (17)$$

where T_0 is the ambient temperature and L is the feed loss:

$$T_{EX} = \int_0^{4\pi} T_B \cdot P(\Theta)\, d\Omega \Big/ \int_0^{4\pi} P(\Theta)\, d\Omega. \qquad (18)$$

T_B is the sky noise temperature and $P(\Theta)$ is the radiation power pattern of the antenna and $d\Omega$ is the unit solid angle. Letting P_i represent the power within the solid angle $d\Omega_i$, Eq. (18) is rewritten as,

$$T_{EX} = \Sigma T_{EXi}, \tag{19}$$

where

$$T_{EXi} = \int_{\Omega_i} T_B \cdot P_i d\Omega_i \Big/ \int_{\Omega_i} P_i d\Omega_i \tag{20}$$

Thus, using Eqs. (19) and (20), T_{EX} is divided into several external noise factors, T_{EXi}, related to antenna efficiencies. Letting the total energy equal unit, as

$$\sum_i \int_{\Omega_i} P_i d\Omega_i = 1 \tag{21}$$

and external noise temperature T_{EX} is rewritten as

$$T_{EX} = \frac{1}{4\pi} \Sigma P_i \int_{\Omega i} T_B \cdot d\Omega_i$$

$$= \Sigma P_i \left(\frac{1}{4\pi} \int_{\Omega_i} T_B \cdot d\Omega_i \right) = \Sigma P_i T_{Bi} \tag{22}$$

where T_{Bi} is defined as the equivalent brightness temperature.

If the antenna efficiency elements and the equivalent brightness temperatures at angles observing their energy are known, external noise temperature T_{EX} can be calculated with considerable accuracy.

Antenna noise temperature T_A at 4.0 GHz was calculated and is summarized in *Figure 13*.

6 Measured Antenna RF Performance

61 97 Feet Cassegrain Antenna

This section summarizes the measured RF performance of the yoke-and-tower type cassegrain antenna using the corrugated horn-reflector primary feed.

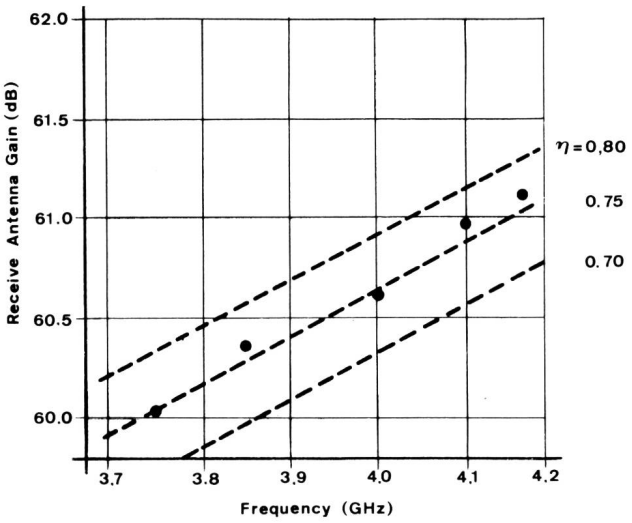

Fig. 14
Measured receive antenna gain
1) 97 ft shaped reflector cassegrain antenna
2) At interface flange of receive port of feed and LNA
3) ICSC/T-23-16E W/1/68 was used for correction factor of the radio star CAS-A for measurement

The first antenna of this type was built at Leuk in Switzerland. Its main reflector diameter is 97 ft.

The main reflector surface of this antenna was assembled with aluminum panels stretch-formed by the Androforming process. The subreflector, which was made from plastic, was so aligned at the main reflector focal point as to establish a high efficiency shaped cassegrain geometry, using a theodolite.

The corrugated horn-reflector was aligned at the predetermined position within the allowance of ±0.1 degree inclination and ±3 mm translation.

The antenna RF performances were measured on site to verify the analysis.

62 Receive Gain and G/T

G/T and receive gain were measured by means of a Y factor method, using the radio star Cassiopeia-A (CAS-A). However, as this earth station is surrounded by a high terrestrial horizon, direct measurement of G/T at a low elevation angle could not be carried out. The receive gain was calcu-

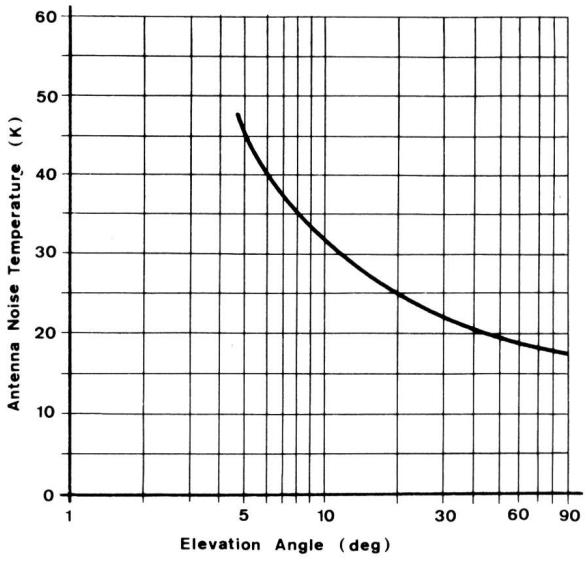

Fig. 13
Noise temperature of 97 ft antenna
(Frequency 4.0 GHz)

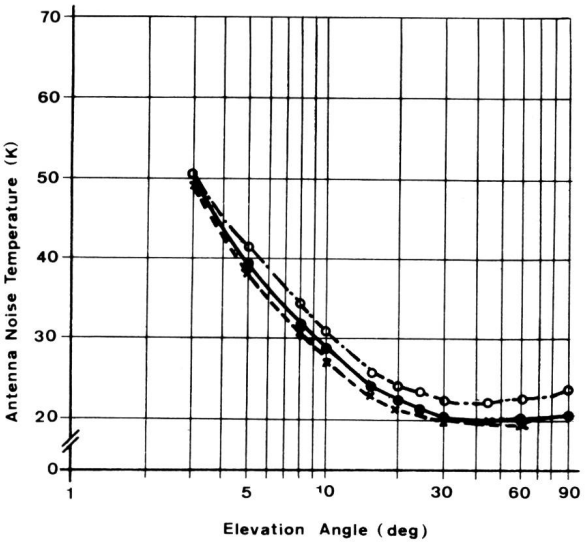

Fig. 15
Antenna noise temperature, measured at the output port of the feed
--o--o-- 3.75 GHz —o—o— 4.00 GHz --x--x-- 4.175 GHz

lated from the measured results of G/T and the antenna noise temperature along the radio star orbit. The antenna noise temperature vs. elevation angle was measured independently at another azimuth direction where the terrestrial horizon is cleared. The measured receive gain vs. frequency is provided in *Figure 14*, and the antenna noise temperature vs. elevation angle is shown in *Figure 15*.

Table III provides the radio star CAS-A parameters, including flux density for the calculation of G/T and receive gain. The measured gain at 4.0 GHz is 60.6 dB at the output flange of the feed, and the total antenna efficiency is 1.26 dB. Very good agreement has been obtained between the computed and measured efficiency, because the result of the analysis in efficiency by full size model test is 1.14 dB.

Table III. CAS-A parameter

Frequency (GHz)	Power flux density (10^{-23}W/m^2/Hz)	HPBW (min)	Angular spread correction (dB)
3.750	1.044793	9.01	0.332
4.000	0.996068	8.45	0.378
4.175	0.965001	8.09	0.410

Notes:
1) According to ICSC/T-23-16E W/1/68
2) Power flux density values is as of November 1973
3) Correction factor for angular spread was derived from Fig. 7 in ICSC/T-23-16E W/1/68
4) The correction factor for atmospheric absorption is calculated by 0.036/sin Θ_{EL} (dB) where Θ_{EL} is elevation angle

The measured noise temperature vs. elevation angle performance deviates somewhat from the calculated results. Possible causes for the deviation are:

- The antenna is surrounded by a high terrestrial horizon and excess noise from the ground increases at high elevation angle.
- The antenna is constructed on a high altitude site (932 m above sea level) and atmospheric absorption decreases at low elevation angle.

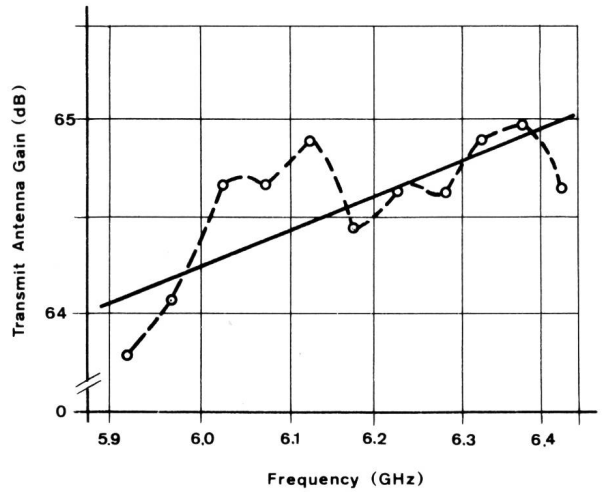

Fig. 16
Measured transmit antenna gain
1) 97 ft shaped reflector cassegrain antenna
2) At interface flange of transmit port of feed and waveguide run from HPA
—o—o— Measured by basic transmission method
——— Average gain

63 Transmit Gain

The transmit antenna gain was also measured by the basic transmission method using a collimation tower 32 km away from the earth station. The correction factor due to the near field effect is added to the measured raw data to obtain the *Fraunhofer* gain.

The result is provided in *Figure 16*. The measured efficiency also has good agreement with the theoretical analysis obtained from the full-size test.

Thus, it is established that the corrugated horn-reflector feed yields the high efficiency characteristics in broadband to the cassegrain antenna.

64 Scattering from Subreflector

The scattering field from the subreflector was also measured on site to verify the theoretical analysis described in subsection 51.

The scattering field from the subreflector was picked up on the main reflector surface, sliding a horn antenna of about 7 dB gain. The measurements were taken at 3.95 GHz and 6.175 GHz. These patterns were geometrically projected on the antenna aperture along the rays of cassegrain geometry.

The results are given in *Figures 17* and *18*.

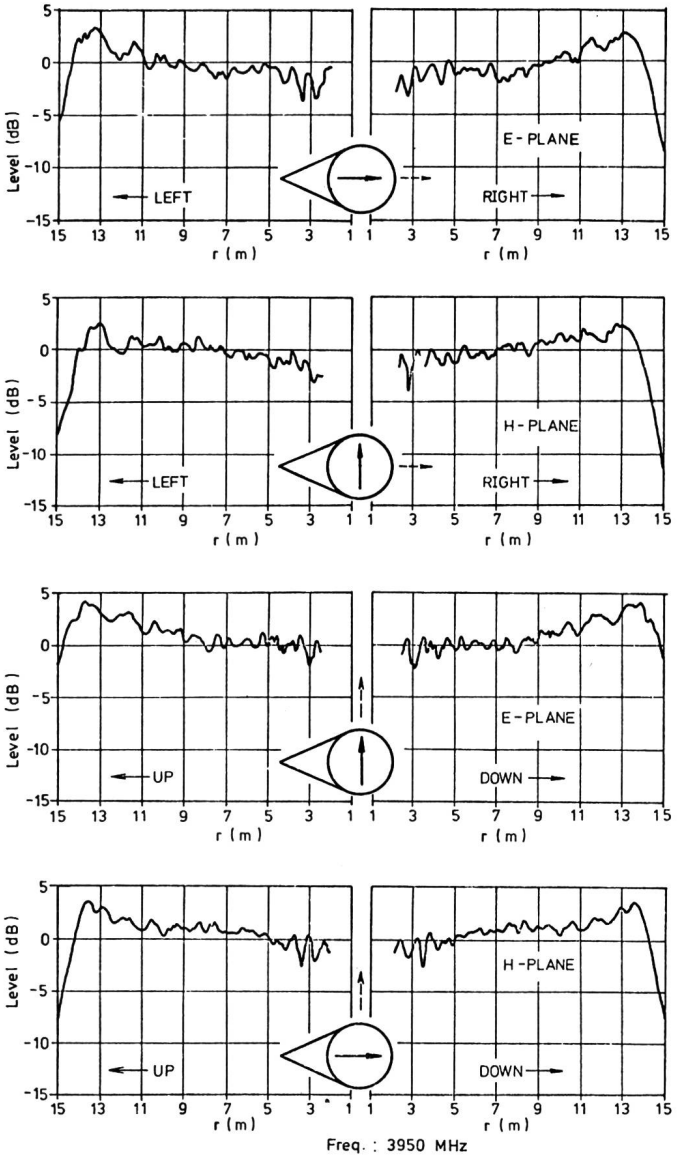

Fig. 17
Measured aperture distribution
Frequency 3,950 MHz

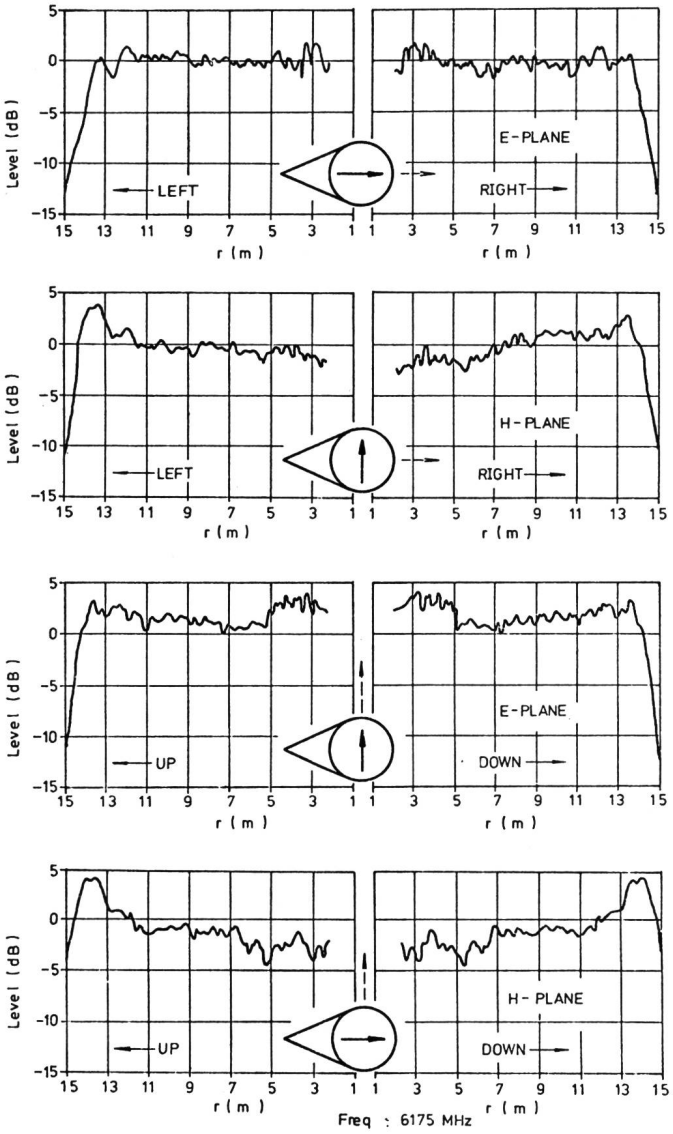

Fig. 18
Measured aperture distribution
Frequency 6,175 MHz

The measured scattering patterns show good agreement with the theoretical analysis and remind us of high efficiency and low noise characteristics of this antenna.

65 Cross Polarization Discrimination

The highlight of this site verification was the measurement of the antenna cross polarization discrimination to investigate the possibility of application, to the future frequency reuse systems, of dual polarization usage.

The measurements were taken in linear polarization mode at the ideal frequencies of axial ratio of the polarizer. The typical pattern at 3.950 MHz is given in *Figure 19,* showing a good agreement with the theoretical analysis of the corrugated horn-reflector feed. It can be said that the measured cross polarization products are almost equal to those of the corrugated horn-reflector feed, since the cross components produced by the concave main reflector are almost eliminated by the convex subreflector in cassegrain system. The 6 GHz measurements were almost identical with the calculated values for the corrugated horn-reflector feed.

These results indicate that the cross polarization isolation for frequency reuse will be of the order of 35 dB, if the tracking accuracy of such an antenna is maintained within 0.1 beam width at 4 GHz.

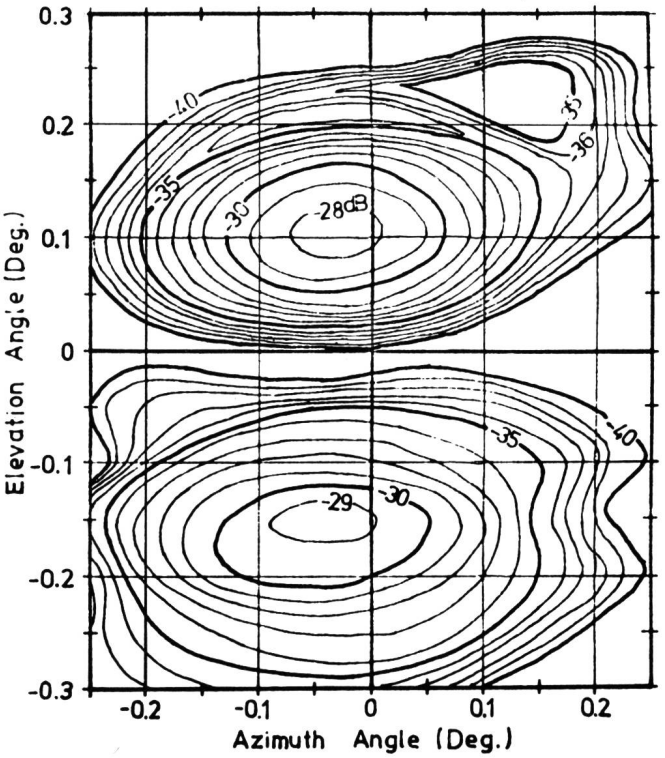

Fig. 19
Measured antenna cross polarization pattern
Frequency 3,950 MHz

66 Other Performances

RF performances of this antenna actually measured on site are summarized in *Table IV*.

The transmit and receive patterns were measured by using the boresite and Intelsat IV. *Figure 20* shows the measured radiation pattern using the beacon frequency of Intelsat IV. *Figure 21* shows the transmit pattern at 6.175 MHz measured by using the boresite 32 km away from the earth station antenna. Side-lobe performances, such as 1st, one degree and back-lobes, satisfy the ICSC Mandatory Items. The wide angle patterns at 3.950 MHz and 6.175 MHz are shown in *Figure 22* and *Figure 23.*

7 Conclusions

The electrical performance of the horn-reflector was improved by corrugating its conical section. It was theoretically and experimentally confirmed that the corrugated conical horn-reflector improves the aperture efficiency and noise temperature of a near field cassegrain antenna; furthermore,

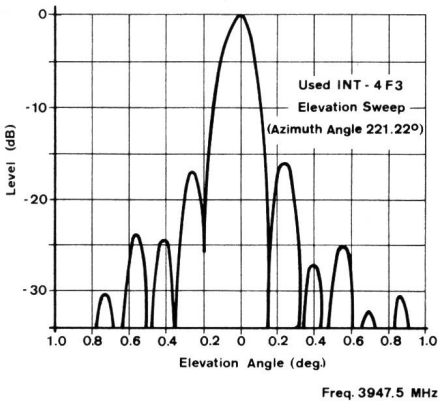

Fig. 20
Receive antenna side-lobe pattern
Frequency 3,947.5 MHz

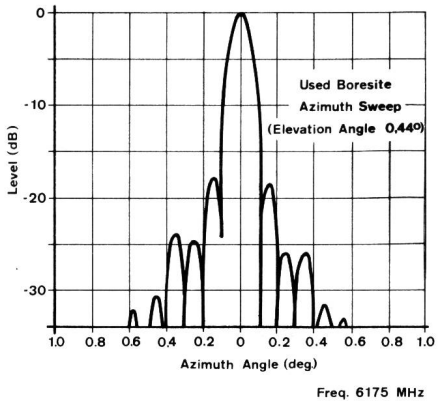

Fig. 21
Transmit antenna side-lobe pattern
Frequency 6.175 MHz

this antenna type can be used in the future frequency reuse system Intelsat V by replacing the present polarizer and duplexer with the high performance polarizer and ortho-mode transducer.

Table IV. Measured antenna performances

Frequency		4.000 GHz	6.175 GHz
Receive System G/T at 5° Elevation Angle		43.1 dB/K*	–
Antenna Gain including Feed Loss		60.6 dB*	64.4 dB**
Antenna Aperture Efficiency		79 %*	77 %**
Antenna Noise Temperature*	at El Angle 5°	39.5 K	–
	at EL Angle 10°	30.0 K	
	at EL Angle 30°	21.7 K	
	at EL Angle 90°	20.8 K	
Antenna Half Power Beam Width		0.150°	0.105° ***
First Side Lobe Level		17.8 dB	17.8 dB***
Wide Angle Side Lobe Level		less than (32–25 log ⌀) dB*** (⌀ is angle measured from main beam.)	
Loss of Feed		0.20 dB	0.10 dB

Notes:
* Measured using CAS-A
** At transmit port input of feed
*** Measured using collimation tower 32 km way from earth station

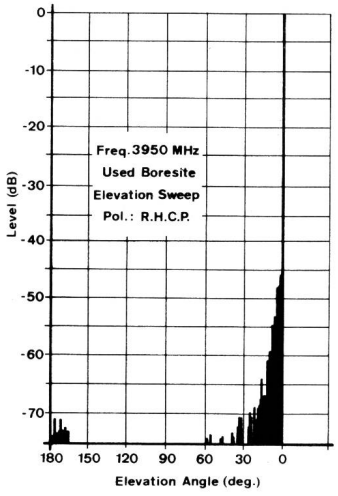

Fig. 22
Wide angle radiation pattern
Frequency 3.950 MHz

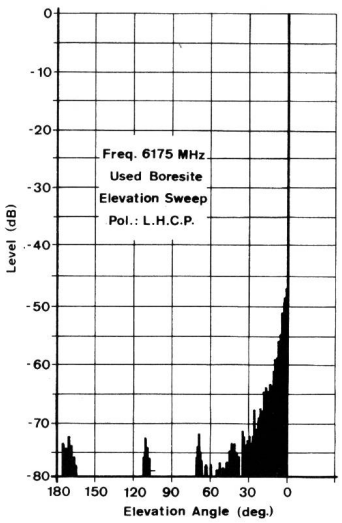

Fig. 23
Wide angle radiation pattern
Frequency 6.175 MHz

Acknowledgment

The authors would like to express their appreciation to Mr. *C. Steffen*, Mr. *P. Breu* and Mr. *P. Hügli* of the Swiss PTT for their technical cooperation throughout this project. The development of the 97 ft antenna reported is the result of the effort of many engineers in the Antenna System Development Department of the Microwave and Satellite Communications Division NEC, Tokyo, and was conducted under the strong leadership of Dr. *T. Kawahashi*, along with the cooperation of many other people in the company.

References

[1] *Trentini G.V., Romeiser K.P.* und *Jatsch W.* Dimensionierung und elektrische Eigenschaften der 25-m-Antenne der Erdefunkstelle Raisting für Nachrichtenverbindungen über Satelliten. Frequenz 19 (1965), S. 402...421.

[2] *Potter P.D.* A New Horn Antenna with Suppressed Sidelobes and Equal Beamwidths. The Microwave Journal (1963, June), pp. 71...78.

[3] *Clarricoats P.J.B.* and *Saha P.K.* Propagation and radiation behaviour of corrugated feed. Part 1: Corrugated-waveguide feed. Proc. IEE, vol. 118 (Sept., 1971) No. 9, pp. 1167...1176.

[4] *Silver S.* Microwave Antenna Theory and Design. McGraw-Hill (1949).

[5] *Hines J.N.* The Electrical Characteristics of the Conical Horn-Reflector Antenna. BSTJ 42 (July, 1963), pp. 1187...1211.

[6] *Bryant G.H.* Propagation in Corrugated Waveguides. Proc. IEE, vol. 116 (Feb., 1969), pp. 203...213.

[7] *Hogg D.C.* Effective Antenna Temperature due to Oxygen and Water Vapour in the Atmosphere. JAP 30 (Sept., 1959) No. 9, pp. 1417...1419.

[8] *Chen S.N.C.* and *Peake W.H.* Apparent Temperature of Smooth and Rough Terrain. IRE (Nov., 1961).